Journal of Atmospheric and Solar-Terrestrial Physics xxx (2017) 1–16

Contents lists available at ScienceDirect

Journal of Atmospheric and Solar-Terrestrial Physics

journal homepage: www.elsevier.com/locate/jastp

Empirical model of TEC response to geomagnetic and solar forcing over Balkan Peninsula

P. Mukhtarov, B. Andonov, D. Pancheva *

National Institute of Geophysics, Geodesy and Geography, Bulgarian Academy of Sciences, Sofia, Bulgaria

ARTICLE INFO

Keywords:
Total electron content (TEC)
TEC response to external forcing
GNSS
Balkan Peninsula

ABSTRACT

An empirical total electron content (TEC) model response to external forcing over Balkan Peninsula (35°N-50°N; 15°E-30°E) is built by using the Center for Orbit Determination of Europe (CODE) TEC data for full 17 years, January 1999 - December 2015. The external forcing includes geomagnetic activity described by the K_p-index and solar activity described by the solar radio flux F10.7. The model describes the most probable spatial distribution and temporal variability of the externally forced TEC anomalies assuming that they depend mainly on latitude, K_p-index, F10.7 and LT. The anomalies are expressed by the relative deviation of the TEC from its 15-day mean, rTEC, as the mean value is calculated from the 15 preceding days. The approach for building this regional model is similar to that of the global TEC model reported by Mukhtarov et al. (2013a) however it includes two important improvements related to short-term variability of the solar activity and amended geomagnetic forcing by using a "modified" Kp index. The quality assessment of the new constructing model procedure in terms of modeling error calculated for the period of 1999–2015 indicates significant improvement in accordance with the global TEC model (Mukhtarov et al., 2013a). The short-term prediction capabilities of the model based on the error calculations for 2016 are improved as well. In order to demonstrate how the model is able to reproduce the rTEC response to external forcing three geomagnetic storms, accompanied also with short-term solar activity variations, which occur at different seasons and solar activity conditions are presented.

1. Introduction

Geomagnetic storms are associated with high-speed plasma injected into the solar wind from coronal mass ejections or coronal holes that impinges upon Earth's geomagnetic field. If the interplanetary magnetic filed (IMF) B_z has southward direction then the solar wind energy enters the magnetosphere-ionosphere-thermosphere system by establishing an interconnection between the southward IMF and the Earth's magnetic field lines. As a result the geomagnetic space environment becomes strongly disturbed and a global ionospheric storm occurs (Kamide and Kusano, 2015). Significant perturbations of the "quiet-time" ionosphere manifested in large variability in the ionospheric density distribution, total electron content (TEC), and the ionospheric current system are observed as a response to the geomagnetic storms. The ionospheric storms of varying degrees are caused by the enhancement of plasma convection, the prompt penetration of high-latitude magnetosphere electric fields, the propagation of disturbance dynamo electric fields to mid-low latitudes, as well as by their combinations (Blanc and Richmond, 1980; Buonsanto, 1999; Schunk and Nagy, 2000; Tsurutani et al., 2004; Mannucci et al., 2008; Heelis et al., 2009). A geomagnetic storm, from the perspective of the upper atmosphere, is a period of intense energy input from the magnetosphere that usually lasts from several hours to a few days. The manifestations of a storm are characterized by a large enhancement of Joule heating leading to significant increase of the neutral gas temperature, raising neutral density via thermal expansion of the atmosphere, and global thermospheric storm winds and composition changes which seriously affect the entire ionosphere (Fuller-Rowell et al., 1994; Rishbeth, 1998; Prölss, 2005).

Much of the interest in understanding the response of the ionosphere to geomagnetic storms has been related to the need of predicting the ionospheric response. This need arises for practical reasons namely the requirement for ground-to-ground communication via the ionosphere using HF radio propagation and from ground-to-satellite through the ionosphere at higher frequencies. Geomagnetic storms have important terrestrial consequences, because many applications such as navigation, satellite communication, remote sensing systems, aircraft detection and tracking and many others rely on radio frequency transmission. All these applications could be seriously affected by strong ionospheric

* Corresponding author.
E-mail address: dpancheva@geophys.bas.bg (D. Pancheva).

https://doi.org/10.1016/j.jastp.2017.11.010
Received 30 July 2017; Received in revised form 17 November 2017; Accepted 19 November 2017
Available online xxxx
1364-6826/

perturbations. Since the last decades, the everyday life of the society has started to depend more on well-functioning communication and navigation systems. As the reliability of most of them can be severely hampered by ionospheric storms, the accurate forecast of these events becomes a required task for mitigating social and economic risks (Borries et al., 2015). Therefore the monitoring, modeling and forecasting of the space weather related ionospheric disturbances are among the important tasks of the ionosphere studies.

The development of the Global Navigation Satellite System (GNSS) during the last two decades has provided a number of possibilities for studying the spatial distribution and temporal evolution of ionospheric electron density disturbances forced by external or internal sources. The GNSS technique has great advantage in producing real-time global and regional ionosphere maps. This has provided opportunity for building global and regional TEC empirical models for prediction. Different regional TEC models have been published in the last decade based on a large variety of methods. Most of them however are background/climatological models (Mao et al., 2008; Kakinami et al., 2009; Feng et al., 2016) which cannot predict the TEC distribution during the geomagnetic storms. Stankov et al. (2004) presented a geomagnetically-correlated forecast TEC model based on the auto-correlation method; it has been tested for 24-h median predictions revealing that the relative errors are larger during night, reaching 10%, but in the rest of the time are varying between 1 and 3%. Andonov et al. (2011) reported a short-term empirical model of the TEC response to the geomagnetic activity over the North American region; it was based on the two-dimensional (2D) cross-correlation analysis which revealed both positive and negative phases of response with respect to the mean state. Most common short-term prediction TEC models are based on the neural network analysis (Tulunay et al., 2006; Maruyama, 2007; Leandro and Santos, 2007; Habarulema et al., 2010, 2011; Huang and Yuan, 2014); they usually predict the TEC value 1 h ahead. Habarulema et al. (2010) developed neural network (NN) based model to follow TEC dynamics over the Southern African region. In order to evaluate the prediction capabilities of the model the results from the NN model have been compared with actual TEC data derived from Global Positioning System (GPS) observations and TEC values predicted by the International Reference Ionosphere (IRI-2007) model during quiet and geomagnetic storm periods. The comparison of the systematic (bias) and root mean squares (RMS) errors of the NN and IRI-2007 models particularly for disturbed conditions indicated that the NN model has better prediction capabilities however its accuracy is still low; particularly for the disturbed period of 28–31 October 2003 (Halloween storms), the RMS error of the NN model changes between 3.45 and 6.61 TECU while those of the IRI-2007 changes from 7.48 to 15.77 TECU. For quiet periods however both models reveal larger *RMS* errors; for example for the period of 16–21 April 2002 the *RMS* errors of the NN model changes between 4.49 and 11.43 TECU while those of the IRI-2007 changes from 4.27 to 22.30 TECU.

Recently Mukhtarov et al. (2013a) built global empirical TEC model response to geomagnetic activity whose mean prediction capabilities assessed by the systematic and RMS errors are −0.20 TECU and 4.59 TECU respectively. These errors are similar to some regional models, as the NN TEC model over Japan (Maruyama, 2007) with a mean RMS error of 4.52 TECU or the NN TEC model over Brasilia (Leandro and Santos, 2007) with a mean absolute error of 3 TECU with standard deviation of 2 TECU. Feng et al. (2016) however pointed out that regional models are necessary especially for certain areas because when global empirical TEC models are built based on global TEC data resource, data with different variations are mixed together causing the deviation in modeling results. Due to this we decided to establish a regional, over Balkan Peninsula, TEC model response to geomagnetic activity using the basic approach of the global model described by Mukhtarov et al. (2013a) and this is the basic aim of the present paper. The geomagnetic activity is described by the K_p-index and the TEC response will be presented as a function of the calendar month, geographic latitude, longitude and LT. The regional TEC model is built using long-term TEC data from 17 years (January 1999–December 2015), obtained from the Center for Orbit Determination of Europe (CODE) (Schaer, 1999). The model approach in the present study is generally similar also to that shown in Andonov et al. (2011) but with a significant improvement related to the solar activity. It has been found that both the regional (Andonov et al., 2011) and global (Mukhtarov et al., 2013a) TEC models do not describe well the ionospheric response when the geomagnetic storm is accompanied with solar activity disturbances, such as fast fluctuations of solar irradiance level presented by solar radio flux F10.7. In order to overcome this weak point of the previously built TEC models we present this regional model where the impact of both geomagnetic and short-term solar variability is included as an external forcing.

2. TEC data set

The regional TEC model is constructed on the basis of vertical TEC maps generated by the CODE center at Astronomical Institute of the University of Bern, Switzerland (http://www.aiub.unibe.ch/research/code__analysis_center/index_eng.html). We note that in this paper TEC everywhere means vertical TEC. For the current study we used data for full 17 years, which span one and a half solar cycles, from 1 January 1999 to 31 December 2015, obtained from the CODE FTP directory: ftp://ftp.unibe.ch/aiub/CODE/. At CODE the TEC is modelled with a spherical harmonic expansion up to degree of order 15 referring to a solar-geomagnetic reference frame (Schaer, 1999). Some details about the CODE TEC data can be found in Mukhtarov et al. (2013a, 2013b). The used TEC data have a time resolution of 1 h and a grid spacing of 5° x 2.5° in longitude and latitude, respectively with errors of several TEC Units (TECU, 1 TECU = 1 0^{16} el/m^2). It is worth clarifying that the TEC data from 1999 to 2014 have a time resolution of 2 h and the hourly data are obtained by interpolation of the 2-hourly original data. The differences obtained from the comparison between the CODE TEC data with the reference TEC values, provided by dual frequency altimeters on board of TOPEX and JASON satellites (able to work over oceans) for period of time between 2002 and 2007 are the followings: the systematic/bias error is 1.45 TECU, the standard deviation (STD) is 5.14 TEC and the RMS error is 5.35 TECU (Hernández-Pajares et al., 2009). Because the altimeters worked over oceans, the above mentioned comparison could be considered as a pessimistic determination of the global TEC map actual errors, i.e. the mentioned errors should be accepted as the worst ones. This is evidence that the GIM/CODE is regarded as one of the precise TEC maps generated from GNSS observations.

The constructed here TEC model is based on the regional CODE TEC maps over southern Europe covering the following geographic region: longitudes from 15°E to 30°E and latitudes from 35°N to 50°N. Fig. 1 shows the location of the investigated area (shaded); the grid points included in this area are marked by red color. Jee et al. (2010) performed a comprehensive comparison between the CODE and TOPEX/JASON TEC data for the period of time between March 1998 and May 2009 which is directed particularly to clarify where (at which regions) and under what geophysical conditions the CODE TEC data have biggest inconsistency with TOPEX/JASON TEC data. It was noted that the CODE TEC data have higher level of disagreement in the northern high-latitudes (above 60°N) and the southern middle- and high-latitudes regions where the Weddell Sea Anomaly and other longitudinal wave structures are situated. It is worth noting that the differences for the southern middle- and high-latitudes regions, which are mostly occupied by oceans and include very sparse GPS ground stations, are higher than the other regions not only for CODE but for all (ESA, JPL and UPC) TEC centers. Therefore, we underline that the CODE TEC data used for building this regional TEC model are consistent with JASON/TOPEX TEC data and we, therefore, consider them accurate enough for this study.

In this study the geomagnetic activity is defined by the global K_p-index as it characterizes the intensity of geomagnetic activity on a planetary scale. However, the network of magnetometers used to

Fig. 1. Location of the area (shaded) covered by the regional TEC model; the grid points included in this area are marked by red color. (For interpretation of the references to colour in this figure legend, the reader is referred to the web version of this article.)

compute K_p is heavily weighted towards Europe and Northern America, i.e. region we are interested in. The K_p-index data are downloaded from the Space Physics Interactive Data Resource (SPIDR), Boulder, Colorado for the considered period of time. The K_p value at every hour is used in this study as it is obtained by linear interpolation of the 3-h K_p values.

In this regional model the TEC response to the geomagnetic activity is investigated by the relative deviation of the TEC defined as:

$$rTEC(t) = \frac{TEC(t) - TEC_m(UT)}{TEC_m(UT)} \quad (1)$$

where UT is the universal hour corresponding to the moment *t*; the latter is counted from the beginning of the period considered. The terms TEC(t) and TEC_m(UT) represent observed and mean TEC values respectively at a given hour (in UT). In this study, similarly to Mukhtarov et al. (2013a), to obtain TEC_m(UT) we use 15-day moving average assigning its value to the last day of the window, i.e. to the 15th day of the window. We use such an approach in order to be able to use the model for nowcasting or short-term prediction (usually 24 h ahead). The use of rTEC means that we try to predict the relative correction to the 15-day mean values for each hour of the prediction period supposing that these CODE rTEC anomalies are generated mainly by geomagnetic and solar forcing. The reasons for using a 15-day window are described in detail by Mukhtarov et al. (2013a).

The main advantage of using rTEC is connected with removing of the regular diurnal oscillations generated by both diurnal variability of the photo-ionization and atmospheric tides vertically propagated from the lower atmosphere. The TEC behavior can be modelled with the following positive function:

$$1.1 + \cos\left(\frac{2\pi}{T}t\right) \quad (2a)$$

where T – is a fluctuation period and t – is current time (in hours). The amplitude frequency characteristic of the function (1), in period range of 0–36 h, is shown in the left plot of Fig. 2. It is seen that when the period is equal to the diurnal one (24 h) or its harmonics (12, 8, 6, ….) the amplitudes of the this function become zero. The other advantage is that by using rTEC the regular seasonal changes are removed also. This is demonstrated again by the frequency characteristics but calculated in period range of

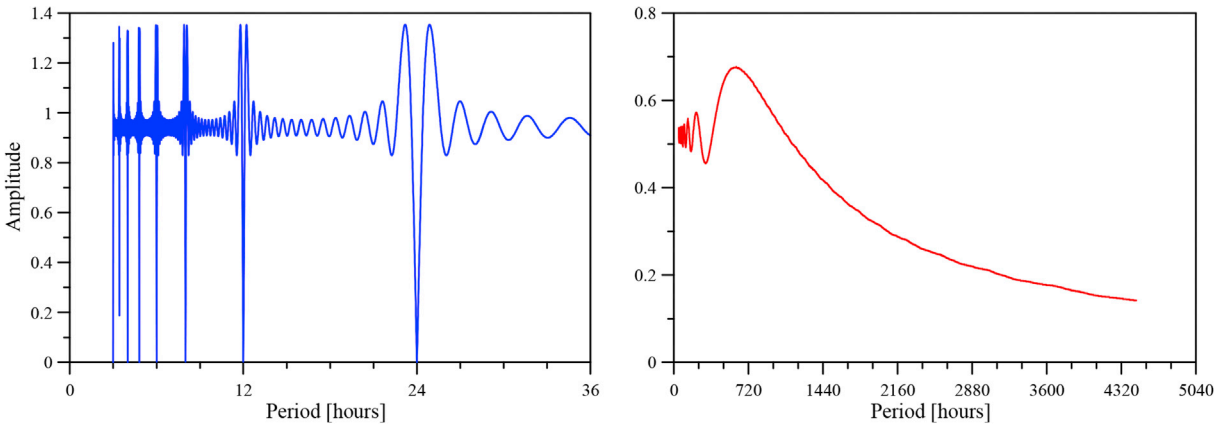

Fig. 2. Frequency characteristics of the used rTEC in the period intervals of 0–36 h (left plot) and 36–4 320 h, i.e. 1.5–180 days (right plot).

1.5–180 days (36–4 320 h) that is displayed in the right plot of Fig. 2. The non-stationary diurnal TEC behavior is described by a modulated trigonometric function with modulation amplitude equal to 0.5:

$$\left(1 + 0.5\cos\left(\frac{2\pi}{T}t\right)\right)\cos\left(\frac{2\pi}{24}t\right) \quad (2b)$$

It is seen that variations with periods larger than 2 months are significantly suppressed. Hence by modeling rTEC using the function (2b) the seasonal and solar cycle variations are effectively filtered while those driven by geomagnetic or variations due to solar rotation, having time scales of days to a month, are not affected and could be investigated and modelled. We note that the time series of rTEC have positive and negative values. The positive (negative) rTEC values correspond to positive (negative) anomaly with respect to the mean TEC calculated from the preceding 15 days. If rTEC is −0.5 (1) this means a double decrease (increase) of TEC.

3. Cross-correlation and regression analyses between *rTEC* and the external forcing defined by K_p-index and *F10.7*

It has been already mentioned that the planetary K_p-index is used as

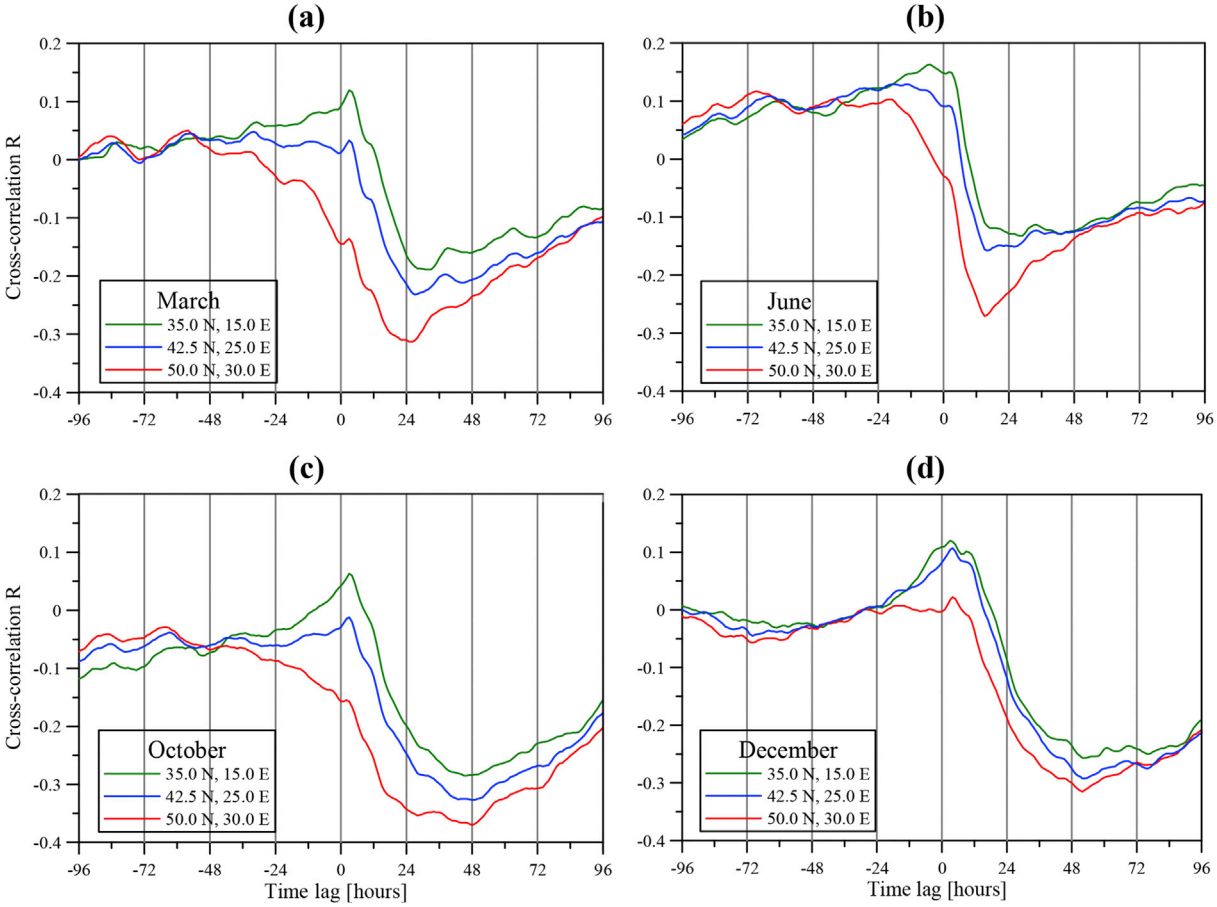

Fig. 3. **(a)** Cross-correlation functions between the Kp forcing and rTEC calculated for March at the following grid points: (35.0°N, 15.0°E; green line), (42.5°N, 25.0°E, blue line) and (50.0°N, 30.0°E, red line); **(b)**, **(c)** and **(d)** The same as (a) but for June, October and December respectively. (For interpretation of the references to colour in this figure legend, the reader is referred to the web version of this article.)

an indicator of the geomagnetic activity because it reflects both the equatorial ring and the auroral currents. Further there are online models for K_p prediction that could be used for implementing online software for producing short-term TEC prediction. The solar forcing is described by solar radio flux F10.7 that is also predicted; the data are downloaded from SPIDR.

The ionospheric response to the geomagnetic activity is a delayed reaction (Muhtarov and Kutiev, 1998; Kutiev and Muhtarov, 2003) that deteriorates the relationship between the K_p-index and the ionospheric anomalies having time scales of days to a month. Investigating the f_oF2 response to the geomagnetic activity by the above mentioned authors the delay has been expressed in terms of the time constant of the cross-correlation function between the relative f_oF2 and K_p-index. This knowledge has been used by Andonov et al. (2011) in constructing the regional TEC model response to the geomagnetic activity for the North American sector. The two-dimensional (2D) cross-correlation analysis revealed that the TEC response is composed of two positive and negative phases which have different duration and time delay with respect to the geomagnetic activity, season and geographical latitude.

In this work we start also with cross-correlation analysis between rTEC and K_p-index calculated for each month of the considered period (1999–2015) because the TEC response is seasonally dependent. Fig. 3 displays the cross-correlation functions between the K_p-index and rTEC for only four months presenting each season; spring month March is shown in (a), summer month June in (b), autumn month October in (c) and winter month December in (d). The results for the following grid points are shown: (35.0°N, 15.0°E; green line), (42.5°N, 25.0°E, blue line) and (50.0°N, 30.0°E, red line), which are chosen to describe two border and one central grid points in the selected region. All cross-correlation coefficients are significant at 99.9% level. The cross-correlation analysis clearly reveals a positive and negative phases of the response which have different duration and time delay with respect to the geomagnetic storm. The two delay parameters indicate seasonal and latitudinal dependence. The TEC response of the most northern latitude, 50°N, except in winter has usually only negative phase. The seasonal dependence of the TEC response to geomagnetic storms is characterized by predominantly positive response in winter with a short (a few hours) time delay as well as mainly negative response in summer with a longer time delay of ~12–14 h. The responses in March and October are closer to the winter one however the duration of the positive phase is shorter.

The external forcing includes besides geomagnetic activity also the short-term variability of solar radiation that can be described by the solar radio flux F10.7. In order to remove the longer period variability we consider the solar forcing in a way similar to rTEC, i.e. define it as:

$$rF107 = \frac{F107 - F107_m}{F107_m} \tag{3}$$

where $F107_m$ is the mean value calculated from the preceding 15 days. The relationship between the rTEC and *rF107* is studied by a group regression analysis performed on the data for the entire time interval of 1999–2015. It is worth reminding that the purpose for using the group regression is to equalize the 'weight' of the cases with significant deviations from the mean state, which are usually small number. The results for the grid point (42.5°N, 25.0°E) are presented in Fig. 4a (black line). Similar results are obtained for the other grid points as well. The best approximation of the obtained group regression is a parabola shown by a red line in the plot that is very close to a linear function. The result of the group regression analysis indicates that the rTEC fluctuations due to the solar variability forcing can be described by a quadratic function of rF107.

4. Basic approach of the model construction

The basic idea of each empirical TEC model which describes the response to the external (geomagnetic and solar variability) forcing is to define a set of analytical expressions which describe the most probable TEC values for given parameters of the external forcing, day of the year, geographic location and LT. It has been already mentioned that the ionospheric response particularly to geomagnetic activity is a delayed process that can be satisfactorily modelled by assuming that the geomagnetic influence is imposed on the inertial system described by an inhomogeneous differential equation of the first order (Kutiev and Muhtarov, 2003). The presence of two phases, positive and negative, of the TEC response shown in Fig. 3 imposed the implementation of two different time delay constants in order to properly describe the two different delayed reactions.

If we assume that the impact of the geomagnetic activity on the TEC can be described by two mechanisms with different time delay constants, T_1 and T_2, then the variability of rTEC can be presented as follows:

$$rTEC(t) \approx \left(f_{T1}\left(K_{pi}(t,T_1)\right) + f_{T2}\left(K_{pi}(t,T_2)\right)\right) f_f(rF107) f(LT) \tag{4}$$

where the function $f_F(rF107)$ describes the solar variability forcing while *f(LT)* represents the dependence of the response on the LT at equal other

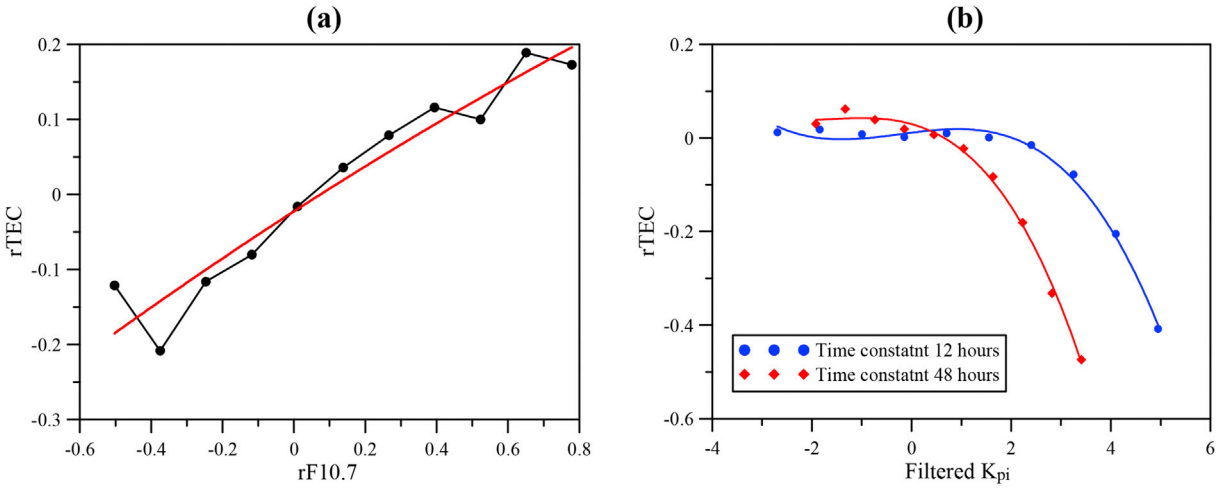

Fig. 4. **(a)** Group regression between the rTEC for the grid point (42.5°N, 25.0°E) and the rF107 (black line) and its approximation with a parabola (red line); **(b)** Group regression between the rTEC for the above mentioned grid point and the filtered K_{pi} for two time constants: 12 h (blue points and line) and 48 h (red squares and line) and their approximation with cubic functions. The calculations are accomplished for the entire time interval (1999–2015). (For interpretation of the references to colour in this figure legend, the reader is referred to the web version of this article.)

conditions. The parameters $K_{pi}(t, T_1)$ and $K_{pi}(t, T_2)$ are the modified with time delay constants respectively T_1 and T_2 values of the K_p-index. These modified parameters are solutions of the first-order inhomogeneous differential equations that could be found in Muhtarov et al. (2002), Andonov et al. (2011), Mukhtarov et al. (2013a) and their final forms are:

$$K_{pi}(t,T_1) = \frac{1}{T_1}\int_{-\infty}^{t}\exp\left(-\frac{t-\tau}{T_1}\right)K_p(\tau)d\tau$$
$$K_{pi}(t,T_2) = \frac{1}{T_2}\int_{-\infty}^{t}\exp\left(-\frac{t-\tau}{T_2}\right)K_p(\tau)d\tau \quad (5)$$

The above presented solutions of the two modified parameters clearly reveal that the transformation of the K_p-index is accomplished only on the basis of values before the current moment t, i.e. known values. In the present study we use additionally filtered values of the integrated K_p-index (K_{pi}) obtained by removing from each value the mean one for the preceding 15 days. In this way the geomagnetic forcing becomes positive or negative with respect to mean state defined for the preceding 15 days, i.e. similar to rTEC.

In order to define the type of the functions f_{T1} and f_{T2} which determine the geomagnetic forcing from (5) we perform again a group regression analysis between the rTEC and the filtered K_{pi} accomplished again for the entire time interval. The results for the grid point (42.5°N, 25.0°E) and for two time constants: 12 h (blue points) and 48 h (red squares) are shown in Fig. 4b. The blue and red lines present their approximation with cubic functions.

Having in mind that the dependence of the response on the LT can be presented by Fourier series, $f_F(rF107)$ as a quadratic function of rF107, and f_{T1} and f_{T2} as cubic functions of K_{pi}, then the rTEC from (4) can be described as:

$$rTEC(t) \approx \left(a_0 + a_1 rF107(t) + a_2 rF107(t)^2\right)\times$$
$$\left(b_0 + b_1 K_{pi}(t,T_1) + b_2 K_{pi}(t,T_1)^2 + b_3 K_{pi}(t,T_1)^3 + b_4 K_{pi}(t,T_2) + b_5 K_{pi}(t,T_2)^2 + b_6 K_{pi}(t,T_2)^3\right)\times$$
$$\left(c_0 + \sum_{k=1}^{4} c_k \cos\left(k\frac{2\pi}{24}\varphi_k\right)\right) \quad (6)$$

We note that the Fourier time series includes the contribution of four harmonics, 24, 12, 8 and 6 h. The number of the included components is defined experimentally; we confined our choice on four diurnal components only because the addition of more components leads to a minor error improvement.

The model function (6) is used to describe rTEC at each grid point included in the considered area in order to study the regional features as accurately as possible. The next step is to determine the constants (a_i, b_i and c_i) of the model (6) under condition that the ranges of the change of the two time constants T_1 and T_2, which defined the delayed geomagnetic response, are known in advance. The determination of the constants a_i, b_i and c_i and the values of the time constants T_1 and T_2 is a nonlinear optimization task that has been solved by applying the "trial-and-error" method in a way that the best approximation in a sense of minimum least square deviation is assured. The details about using this method can be found in Andonov et al. (2004) and Mukhtarov et al. (2013a).

An assessment of the proposed empirical model performance has been performed by calculating the differences between experimental and modelled TEC values. The statistics of the differences for the entire data set (1999–2015) will be presented here in terms of the root mean square (*RMS*) error. Fig. 5a displays the longitude-latitude distribution of the RMS error (in TECU). We clarify that the *RMS* errors are determined in each grid point and later the *RMS* map is constructed by interpolation based on the Inverse Distance Method (Shepard, 1968). It is seen that the *RMS* almost does not depend on the longitude and this is best evident at latitude of ~43°N. The *RMS* slightly decreases/increases to the east in the latitude range of (35°N-43°N)/(43°N-50°N). The *RMS* however reveals well expressed latitudinal dependence; it decreases with the increase of the latitude; the *RMS* changes from 3.13 to 2.45 TECU. This latitudinal dependence is expected in advance because it is known from Mukhtarov et al. (2013a) that the largest *RMS*, reaching 7.5 TECU, has been found at low latitudes where the equatorial ionospheric anomaly (EIA) is developed, the crests of which are located at around ±15° from geomagnetic equator.

The overall *RMS* error can be described in details by showing its seasonal dependence. Fig. 6 shows the longitude-latitude distribution of the *RMS* (in TECU) in the following months again presenting different seasons: (a) January; (b) March; (c) July and (d) November. The largest errors are found in the equinoxes where the RMS changes from 2.9 TECU to 3.5 TECU; this certainly is due to both semiannual variations in the ionosphere and semiannual variation in geomagnetic activity. The range of RMS change in summer, (1.85–2.85) TECU, is larger than that in winter, (1.94–2.3) TECU, with bigger differences seen at lower latitudes which depend stronger on the variability of the EIA during geomagnetic storms. It is known that the negative response of the low latitude ionosphere during summer is usually stronger than that in winter because the disturbed wind system has the same direction as the regular thermospheric wind blowing from summer to winter hemisphere.

Fig. 7 displays the longitude-latitude distribution of the RMS error at different times (UT) in order to check how the *RMS* changes during the entire day; the following times are shown (a) 00UT; (b) 06UT; (c) 12UT, and (d) 18UT. As expected, the RMS is proportional to the background TEC and is the smallest during the night (1.34–1.84) TECU (a) and the largest during the day (4.5–5.5) TECU (c), as well as the different directions of the slope of the lines defining the same *RMS*. As always the *RMS* has the largest values at the most southern latitude, 35°N, the slope depends on the LT of the considered longitudes; while at 00UT the electron density increases with moving to the east at 12UT it decreases. The ranges of the *RMS* errors during morning and late afternoon hours are not very different; at 06UT (b) the RMS changes between 2.1 TECU and 3.7 TECU while at 18UT (d) its range is (1.9–3.1) TECU; at 06UT the errors are larger than those at 18UT because in the first case the electron density over the considered area rapidly increases while in the second case these are evening hours with lower electron density.

With additional cross-correlation and regression analyses we would like to shed some light on the type of the discrepancy between the CODE data and the present model. Fig. 8a shows the normalized cross-correlation function between the rTEC CODE data and the rTEC model while Fig. 8b presents the normalized cross-correlation function between the K_p-index and the rTEC CODE data (red line) and between the K_p-index and the difference between the rTEC CODE data and rTEC model (blue line). The calculations are made for the central grid point (42.5°N, 25.0°E) and for all October months of the period 1999–2015. The month of October has been selected as it is the most geomagnetically disturbed month during the considered period. The cross-correlation analysis reveals that practically the impact of the geomagnetic activity on the difference between the rTEC CODE data and rTEC model is absent (Fig. 8b); it is seen that the correlation is almost zero when the time lag is positive

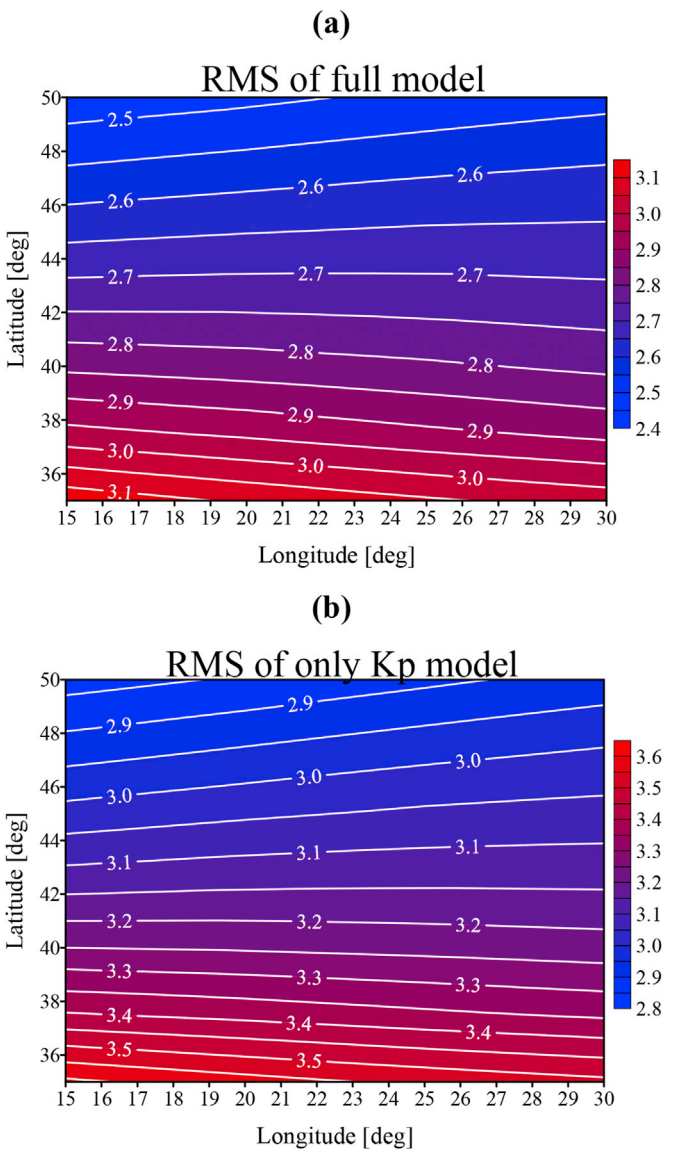

Fig. 5. **(a)** Longitude-latitude distribution of the RMS error (in TECU) calculated from the full model; **(b)** The same as (a) but calculated from only the Kp model.

in comparison with the negative correlation between Kp and the rTEC itself. There is however a diurnal component existing in both rTEC CODE data and rTEC model that is registered not only in Fig. 8a but in their autocorrelation functions as well (not shown result). A diurnal component exists also in the autocorrelation function calculated from the difference between the rTEC CODE data and rTEC model (also not shown). This means that a special function *f(LT)* which has been used in the model to represent the dependence of the response on the LT at equal other conditions most probably does not describe the diurnal variations of rTEC sufficiently well. The fact that a diurnal component exists in the autocorrelation function of the rTEC CODE data also may indicate that this component could not be related to the external forcing of the ionosphere. Fig. 8c presents the regression between the rTEC CODE data and the rTEC model (black line) again for the central grid point (42.5°N, 25.0°E) and for all October months of the period 1999–2015. The real regression is compared with the ideal one, marked by a red line; the comparison shows that the model underestimates the large positive anomalies which appear rarely. The latter is supported by the non-symmetric histogram of the rTEC CODE data displayed in Fig. 8d.

The above presented longitude-latitude distributions of the *RMS* errors during different conditions indicate that the present model shown in Figs. 5–7 quite well describes the ionospheric response to external forcing over the Balkan Peninsula; the errors are significantly lower than the global model errors reported by Mukhtarov et al. (2013a). This means that if there is a regular interest in the ionospheric response over some particular region it would be better a regional model to be constructed and used instead of a global one. These errors are calculated however on the basis of data for the period of 1999–2015 that have been used for generating the model. This is a validation of the self-consistency of the modeling procedure. The real evaluation of a given model has to be done on data which are not included in the construction of the model. For this purpose we calculate the average (bias) and *RMS* of the error for 2016; they are respectively 0.036 TECU, i.e. practically there is no bias, and 1.889 TECU. These small errors indicate that the present regional TEC model is appropriate for short-term prediction of the ionospheric response to external forcing over the considered area. We note however that the quality of the short-term prediction of the ionospheric response to external forcing depends also on the two other models that predict K_p and F10.7. Therefore the building of regional models is really useful work because they are more adaptable in certain areas and give more accurate forecasts for them.

5. Model results

In order to demonstrate how the model is able to describe the rTEC response to geomagnetic activity three geomagnetic storms observed at different seasons and solar activity conditions are studied.

Fig. 9a presents the 3-hourly K_p-index for the period of time 26–31 October 2003; these are famous Halloween storms. On 29 and 30 October three geomagnetic storms were observed as the last two of them were superstorms (Pancheva et al., 2016). The first geomagnetic storm is associated with an abrupt increase of the K_p-index up to 9 at ~0 900 UT on 29 October. The second storm occurs around 2 330 UT on 29 October and K_p-index again is close to 9. The last storm is the most intense and is at 2 315 UT on 30 October and K_p-index again is 9. After the third storm main phase, according to the K_p-index, the October geomagnetic event started to recover as the K_p-index decreases to 3 on 01 November at 12 UT. The plots in the left column of Fig. 9b demonstrate the comparison between the rTEC CODE data marked by blue lines and the rTEC model data marked by red lines. The plots in the right column show the same comparison however between the TEC CODE data and TEC model data. Comparisons in three grid points are presented to demonstrate quite strong latitudinal dependence of the ionospheric response to these geomagnetic storms over Balkan Peninsula and the ability of this model to reproduce correctly the TEC anomalies. The comparison particularly between rTEC model and CODE data reveals the following features (the rTEC scales are the same for all grid points): (i) the Halloween storms take place on 29–30 October however both data and model show three strong positive anomalies before the disturbed period, 26–28 October, which apparently are not driven only by the geomagnetic activity; there are two comparatively weak K_p-index disturbances during the nigh-time 26/27 October and on 28 October during morning and day-time hours which could contribute to delayed responses on 27 and 28 October; (ii) the two geomagnetic storms on 29 October drive two positive rTEC anomalies which are latitudinally dependent particularly the first one (the magnitude of the first anomaly increases with the decrease of the latitude) and are quite well described particularly the second one by the model; (iii) due to the decrease of the K_p-index from 9 to 5 on 30 October a strong negative anomaly is observed reaching a magnitude of ~ -0.6 at lower latitudes that is very well described by the model, and (iv) the most intense geomagnetic storm at the end of October 30 generates strong positive rTEC anomaly observed and modelled only at the highest latitude, 50°N; this anomaly is comparatively well reproduced by the model.

The three positive rTEC anomalies observed on 26–28 October are forced by flare effects, the growth of the X-ray intensity and substorm

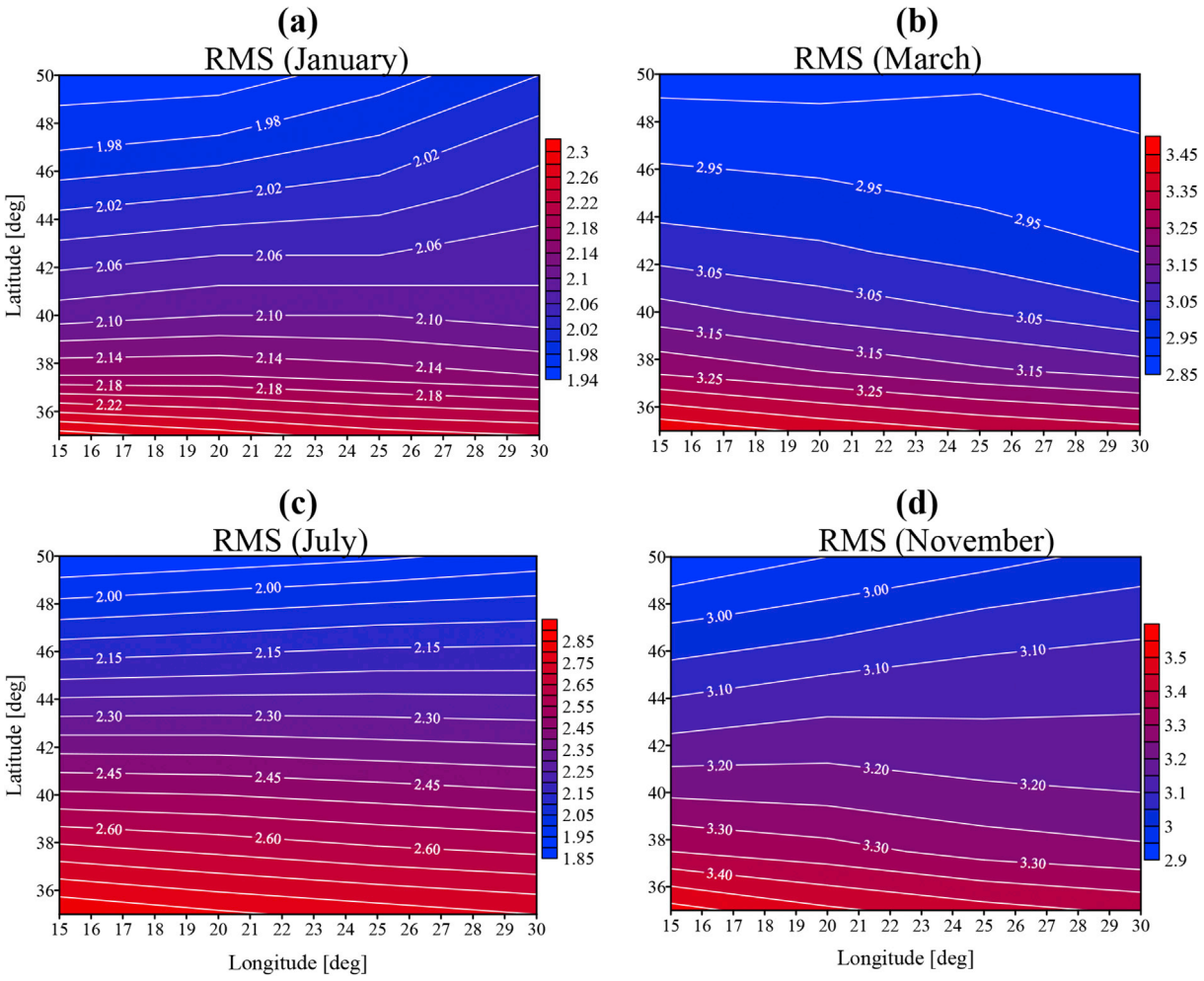

Fig. 6. **(a)** Longitude-latitude distribution of the RMS error (in TECU) in January; **(b)**, **(c)** and **(d)** The same as (a) but for March, July and November respectively.

activities and this issue is described in detail by Blagoveshchenskya et al. (2006). The regional model however describes them very well namely because of the inclusion of the short-term variability of the solar radiation described by *rF10.7* effect. This problem is considered in detail later when the full model is compared with the model where only the K_p effect is included but here we clarify only how *rF10.7* anomaly influences the variability of rTEC. When there is a large *rF10.7* anomaly (as in this case a very strong positive anomaly, with a magnitude of ~0.8 that will be shown later in Fig. 12a) but the geomagnetic activity is not strong then the model output is defined mainly by the first and third terms in the right part of eq. (6), i.e. these are modulated by the solar anomaly diurnal variations of rTEC observed 26–28 October.

The rapid onset and short duration of the positive phase of the rTEC response on the first day-time storm (at ~0 900 UT on 29 October) is most probably forced by the eastward prompt penetration electric field (PPEF) that can strengthen the EIA and expand it poleward with the ionization crests displaced to midlatitudes (Kelley et al., 2004; Mannucci et al., 2005). Due to this process the positive rTEC anomaly is the strongest at lowest considered latitude of 35°N. The decrease of the positive rTEC anomaly during afternoon hours of 29 October could be driven by the westward disturbance dynamo electric fields (DDEF) (Blanc and Richmond, 1980) that dominate the low latitudes with a delay of 4–5 h from the first incidence of the PPEF following the storm onset and have opposite to the PPEF effect. The response to the second geomagnetic storm is observed before its main phase at 2 330 UT on 29 October because the disturbed condition started around 17 UT when the B_z component of the IMF became negative and the D_{st}-index started rapidly to decrease (Lei et al.,. 2014; Fig. 1 there). The equatorial anomaly significantly enhances after 18–19 UT and expands poleward (Lei et al., 2014, Fig. 5 there) probably again due to the PPEF causing the second rTEC positive anomaly on 29 October. The second anomaly has longer duration in the most northern grid-point at 50°N (after midnight) most probably forced by the combined action of plasma accumulation at higher latitudes by the convection electric field (Heelis et al., 2009) that is strengthened and transferred to lower latitudes by the geomagnetically driven equatorward winds (Balan et al., 2011). Due to this the amplitude of the most northern rTEC anomaly (at 50°N) is slightly larger than those at lower latitudes (~0.7 versus ~0.6 seen in the rTEC CODE data). We clarify that the magnitudes of the anomalies are evaluated from their minimum level defined from the first positive response. The negative anomaly is mainly due to the composition changes (Rishbeth, 1991; Prölss, 1995) occurring at high latitudes, i.e. the thermosphere becomes richer in molecular nitrogen and poorer in atomic oxygen, which are transferred to midlatitudes by the geomagnetically driven equatorward winds. The positive rTEC response to the third storm (at 2 315 UT on 30 October) is probably driven by the plasma accumulation by the convection electric field but in this case the high latitude plasma accumulation is transferred by the disturbed winds only to the most northern latitude.

In order to asses how the model reproduces the CODE TEC response to the external forcing on October 26–31, 2003 we calculate the mean and *RMS* errors for each day of the considered period and for the entire area covered by this model; the results are presented in Fig. 9c where the mean error (in TECU) is marked in blue color while the RMSE (in TECU) in red color. It is seen that while at the first day, October 26, both the

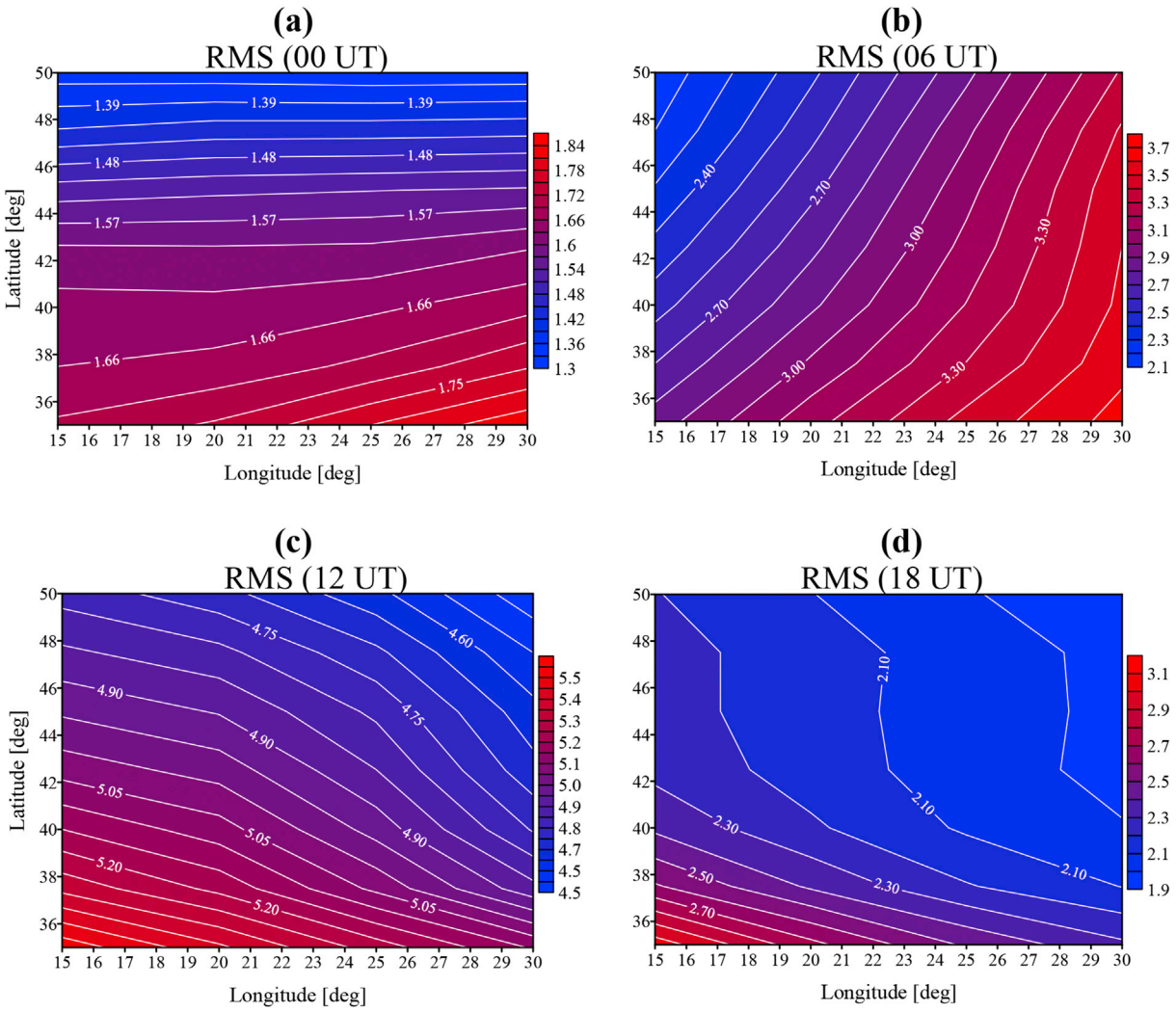

Fig. 7. **(a)** Longitude-latitude distribution of the RMS error (in TECU) at 00UT; **(b)**, **(c)** and **(d)** The same as (a) but at 06UT, 12UT and 18UT respectively.

systematic error (blue color) and *RMSE* (red color) are very small, respectively 0.7 TECU and 1.32 TECU, then the *RMSE* increases reaching maximum values of 3.9 TECU and 3.82 TECU on 28 and 29 October respectfully and gradually decreases to 2.76 TECU on October 31. The systematic errors during the disturbed days 29 and 30 October are respectfully −1.32 TECU and 2.31 TECU revealing that while during the first day the model underestimates the CODE data while the second day it overestimates them; this is well seen in Fig. 9b in both rTEC and TEC data.

The mean and *RMS* errors for the entire considered period are calculated as well and they are respectively 0.55 TECU and 3.28 TECU. These are quite good errors in comparison with the global TEC model (Mukhtarov et al., 2013a) indicating that the model slightly overestimates the anomalies. Summarizing the comparison's result for the Halloween geomagnetic storms we conclude that the model reproduce very well both the period before the storms as well as during the storms regardless the significant latitudinal dependence of the response.

The strongest storm of solar cycle 24 commenced on 17 March 2015 (St. Patrick's Day) and had duration for more than 24 h causing a very strong response of ionosphere. This storm resulted from the interaction of a pair of successive coronal mass ejections (CMEs) on 15 March; the plasma cloud plus the compression of a high-speed solar wind hit the geomagnetic field directly causing substantial plasma precipitation and auroral substorm activities (Astafyeva et al., 2015). Variations of the 3-hourly K_p-index during 15–20 March 2015 are presented in Fig. 10a. The storm sudden commencement was registered at ~04:45 UT on 17 March and the K_p-index reached 5. According to Yao et al. (2016) the development of the storm can be divided into three typical stages: the initial phase (~04:45–07:30 UT), the main phase (~07:30–22:45 UT), and the recovery phase (after 22:45 UT). During the main phase of the storm the K_p-index changes from 5 to almost 8 indicating that the storm reached a strong to severe level. The comparison of the rTEC response in the CODE data and the model is shown in the left column of plots of Fig. 10b while the right column of plots reveals the comparison of the CODE TEC and the modelled TEC. The ionospheric response on March 17 over the Balkan Peninsula is composed of two positive anomalies with the second being stronger. The magnitude of the second anomaly increases with the decrease of the latitude. The model reproduces approximately well only the second anomaly except at latitude of ~50°N where it significantly underestimates its magnitude. This affects the comparison of the TEC in the right column of plots where the disturbed day of March 17 is not reproduced well. The positive TEC anomaly observed during the day-time of March 17 is forced by the eastward PPEF that can strengthen the EIA and expand it poleward with the ionization crests extended to midlatitudes. This result is supported by that reported by Nava et al. (2016) where the two enhancements of the equatorial anomaly March 17 in the African sector, i.e. European as well, can be clearly distinguished as the second enhancement is significantly stronger than the first one (Fig. 4 in Nava et al., 2016). The two peaks are observed most probably because the B_z component of the IMF is negative between

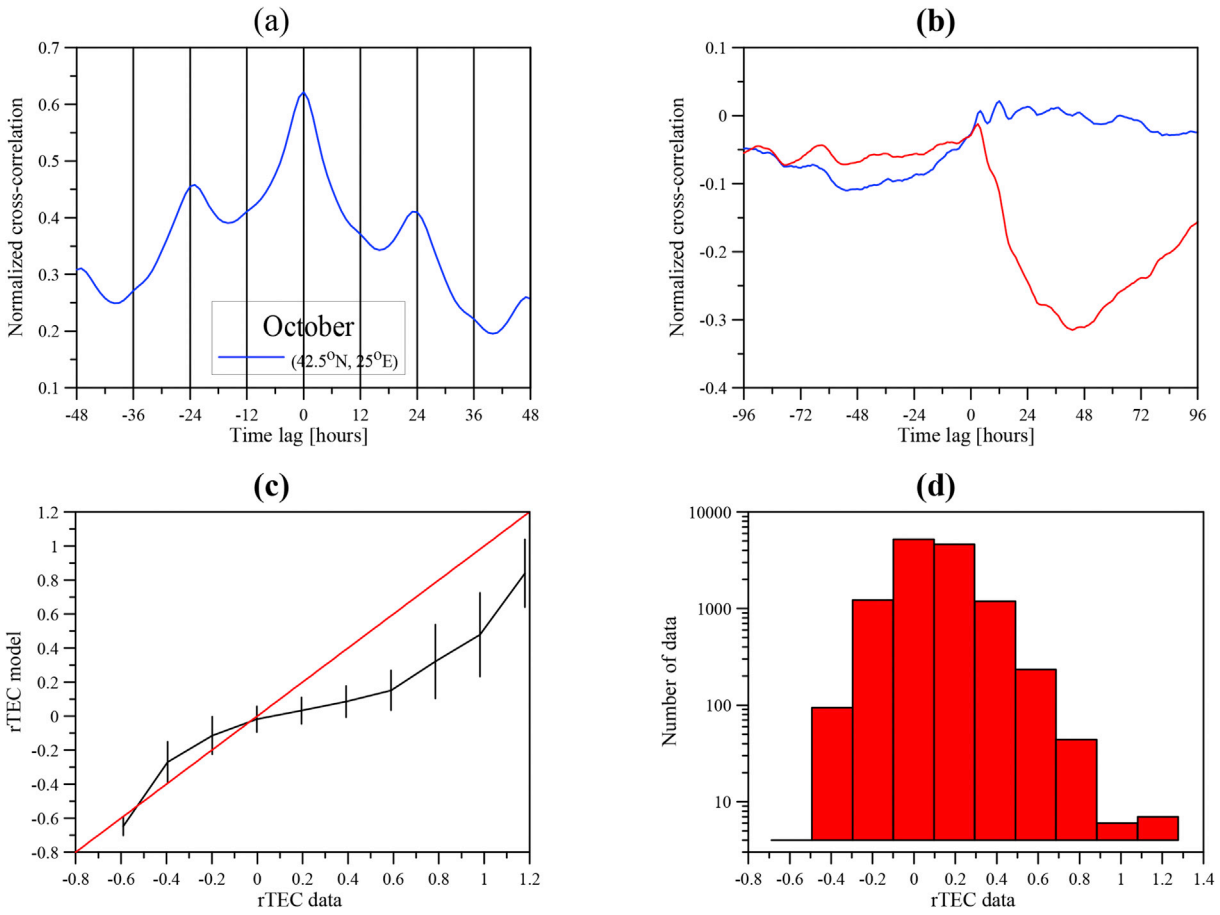

Fig. 8. **(a)** Normalized cross-correlation function between the rTEC CODE data and the rTEC model; **(b)** Normalized cross-correlation function between the Kp and the rTEC CODE data (red line) and between the Kp and the difference between the rTEC model and rTEC data (blue line); **(c)** Regression between the rTEC data and the rTEC model (black line) compared with the ideal regression (red line), and **(d)** Histogram of the rTEC CODE data. The calculations are for the grid point (42.5°N, 25.0°E) and for all October months of the period 1999–2015. (For interpretation of the references to colour in this figure legend, the reader is referred to the web version of this article.)

~06:00–09:30 UT and after ~12:00 UT and only then the eastward PPEF that can affect the ionospheric plasma. During the early night hours of March 18 a strong negative anomaly is observed in both the CODE data and the model driven by the composition changes. The negative rTEC anomaly rapidly decreases during the day-time of March 18 probably forced by some increase of the K_p-index up to 5+. We note that model reproduces quite correctly the negative anomaly and the following rTEC variability.

Fig. 10c presents the mean error (in TECU, blue color) and the RMSE (in TECU, red color) calculated for each day of the considered period, 15–20 March 2015, and for the entire Balkan Peninsula region. It is seen that the strongest systematic and *RMS* errors are observed on March 17 when the geomagnetic storm occurs; they reach values respectively −3.9 TECU, i.e. the model clearly underestimates the CODE data, and 6.5 TECU. These errors are significantly higher than the errors for the other days of the considered period when the systematic error changes between −0.5 TECU and 2.5 TECU while the RMSE between 1.4 TECU and 3.8 TECU.

The calculated systematic and *RMS* errors for the whole period of 15–20 March 2015 and for the entire area covered by this model reveal that they are respectively −0.10 TECU and 3.52 TECU. We note that despite the TEC response to the geomagnetically disturbed day on 17 March has been underestimated the small systematic error is small because there are two days where the model overestimates the data; this is particularly well seen at lower latitudes. Summarizing the comparison's result for the St. Patrick's Day geomagnetic storms on 17 March 2015 we conclude that the model reproduces not very well the positive TEC response on March 17; two positive anomalies were seen in the data but the model predicts only the second one with an underestimated magnitude. The strong negative anomaly followed by variable rTEC response on March 18 is however very well reproduced.

The second largest geomagnetic storm in solar cycle 24 is that observed on 22–23 June 2015. Fig. 11a presents the variation of the 3-hourly K_p-index during 21–26 June 2015. Two CMEs hit the Earth at 0 545 UT and at 1830 UT on June 22 (Astafyeva et al., 2016) giving rise to two enhancements of the K_p-index that reach magnitudes slightly larger than 4 and 8 respectively. The next increase of the K_p-index is around 0 430 UT on June 23 when it approaches 8. This is actually the peak of the main phase of the storm and later the K_p-index gradually decreases. A new increase of the K_p-index is seen between ~05 and 16 UT on June 25 when the K_p-index reaches values between 5 and 6. The comparison between the rTEC CODE (blue line) and model (red line) data are shown in Fig. 11b (left column) while the plots in the right column demonstrate the comparison between CODE TEC and model data. The first K_p peak on June 22 forces a positive rTEC anomaly, observed well in both the data and the model at early afternoon hours. The peak is followed by a very strong negative anomaly that reaches value of −0.65 particularly at latitude of 50°N where it is reproduced perfectly well by the model. There is a weak TEC response to the second K_p peak on June 22, seen mainly at latitude of 50°N before the midnight, that can be distinguished at the base of this negative anomaly. The K_p peak at 04:30 on June 23 drives mainly negative response; the enhanced geomagnetic activity disturbs seriously the normal diurnal course and around noon and early afternoon the rTEC rapidly decreases. The model again describes perfectly well the response during the entire day on June 23. The K_p enhancement on June 25 drives positive anomaly well seen in both the

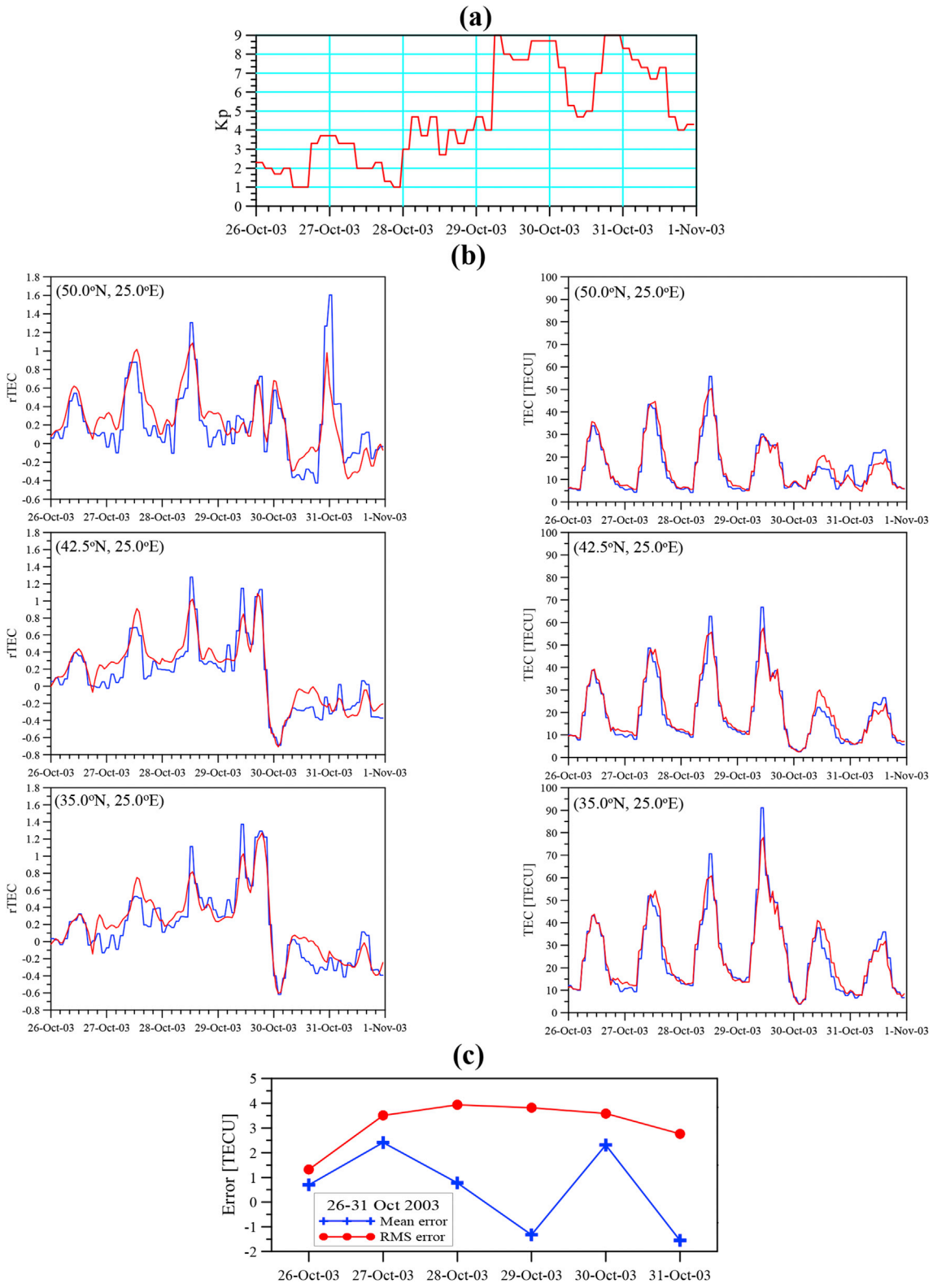

Fig. 9. **(a)** The 3-hourly Kp-index for the period of time 26–31 October 2003; **(b)** (left column of plots) Comparison between the rTEC CODE data (blue line) and the rTEC model (red line) for three grid points shown at the upper left side of the plots; (right column of plots) Comparison between the TEC CODE data (blue line) and the TEC model (red line) for the same grid points, and **(c)** Temporal variability of the mean error (in TECU, blue color) and the RMSE (in TECU, red color) presented for each day of the considered geomagnetic storm. (For interpretation of the references to colour in this figure legend, the reader is referred to the web version of this article.)

data and the model; the predicted magnitude of the positive response however is slightly weaker than that in the data. The mechanisms generating positive day- and nigh-time storm responses as well as the reason for the negative one in this case are the same as those mentioned for the Halloween storms; the very strong negative response here is due to the same direction of both the mean thermospheric winds and the geomagnetically disturbed ones during the summer, i.e. toward the equator.

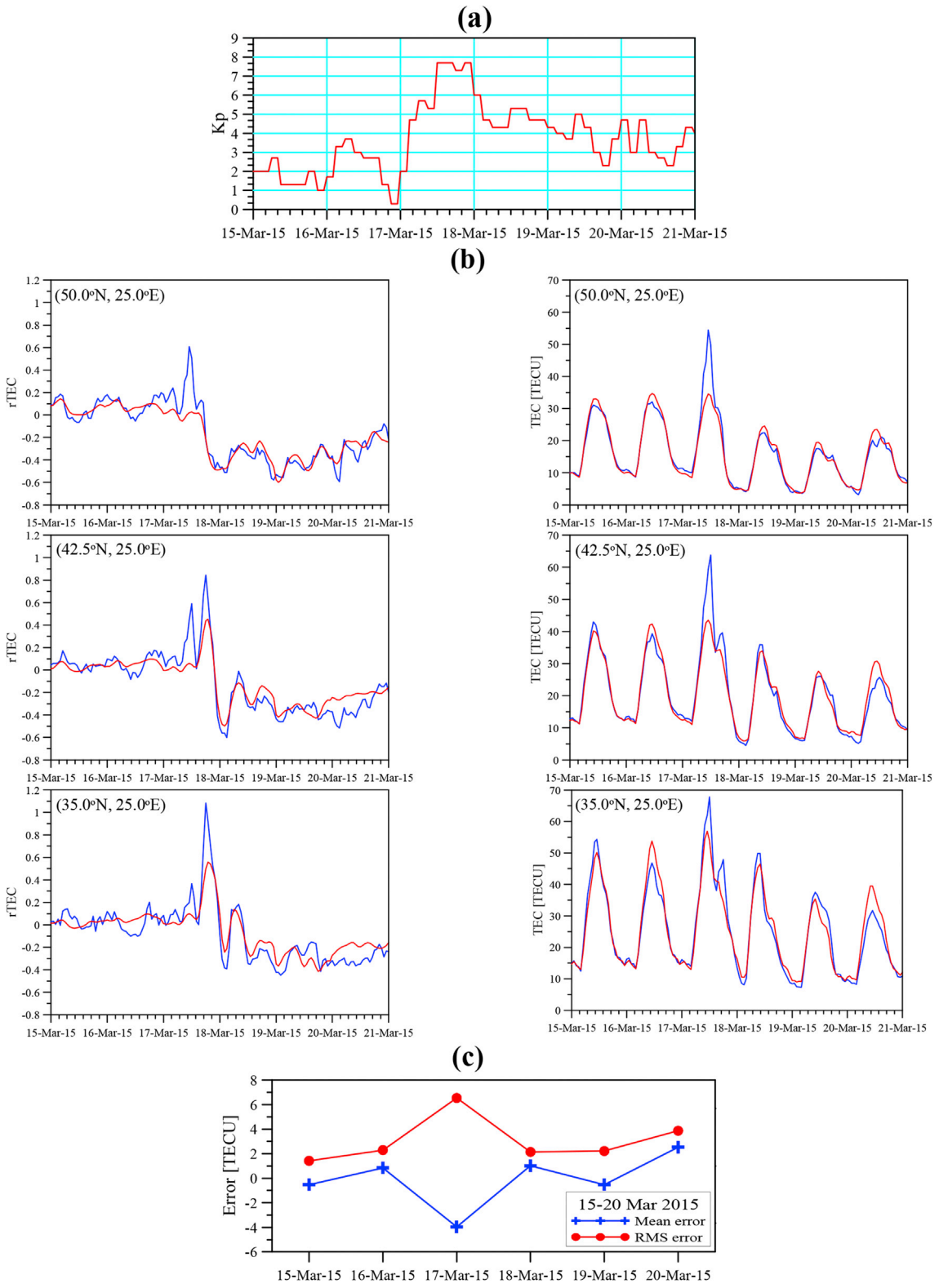

Fig. 10. The same as Fig. 9 but for the period of 15–20 March 2015.

Fig. 11c presents the mean error (in TECU, blue color) and the RMSE (in TECU, red color) calculated for each day of the considered period, 21–26 June 2015, and for the entire Balkan Peninsula region. It is evident that during the disturbed days, 22 and 23 June, both the systematic and *RMS* errors are very small; the systematic error is practically zero (0.02 and 0.04 TECU) while the *RMSE* are respectively 1.26 and 0.95 TECU. This is clear evidence that the regional model reproduces very well these disturbed days. Despite the correctly modelled rTEC response during the disturbed day of 25 June it is seen that the model underestimate the data, the systematic error is −0.98 TECU, while the RMSE reaches 3.5 TECU.

The calculated systematic and *RMS* errors for the whole period of 21–26 June 2015 and for the entire area covered by this model reveal that they are respectively 0.71 TECU and 2.61 TECU. Summarizing we conclude that the 22–23 June 2015 geomagnetic storm exhibits a

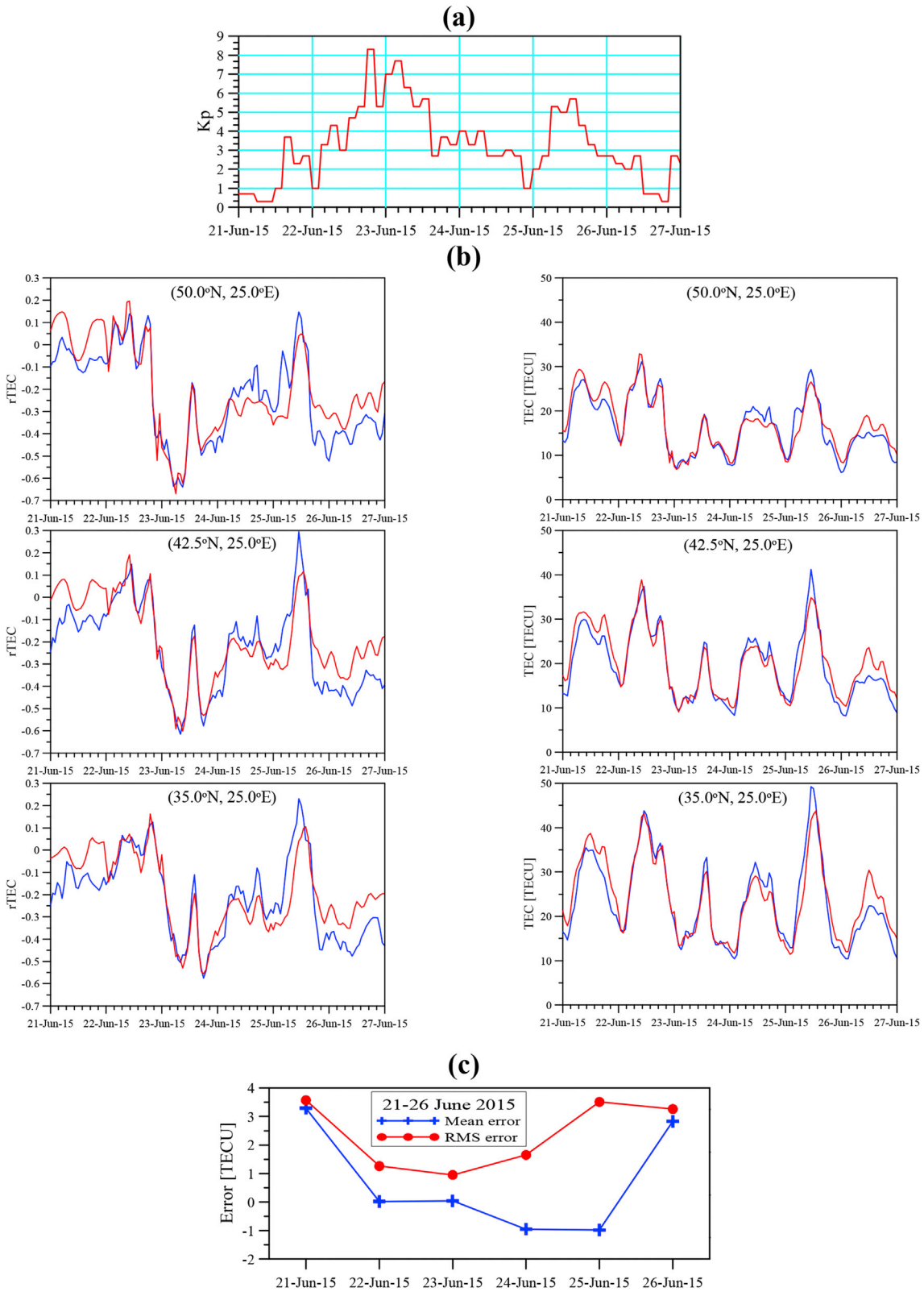

Fig. 11. The same as Fig. 9 but for the period of 21–26 June 2015.

multistep development and is not easy for modeling. The comparison between the CODE and model data shown in Fig. 11 reveals that the ionospheric anomalies seen on 22 and 23 June are perfectly predicted. The strong positive anomaly on 25 June is also well predicted but with smaller amplitude.

6. Summary

This study presents an empirical model of rTEC response to external forcing over Balkan Peninsula. The external forcing includes geomagnetic activity described by the Kp-index and short-term variability of the solar

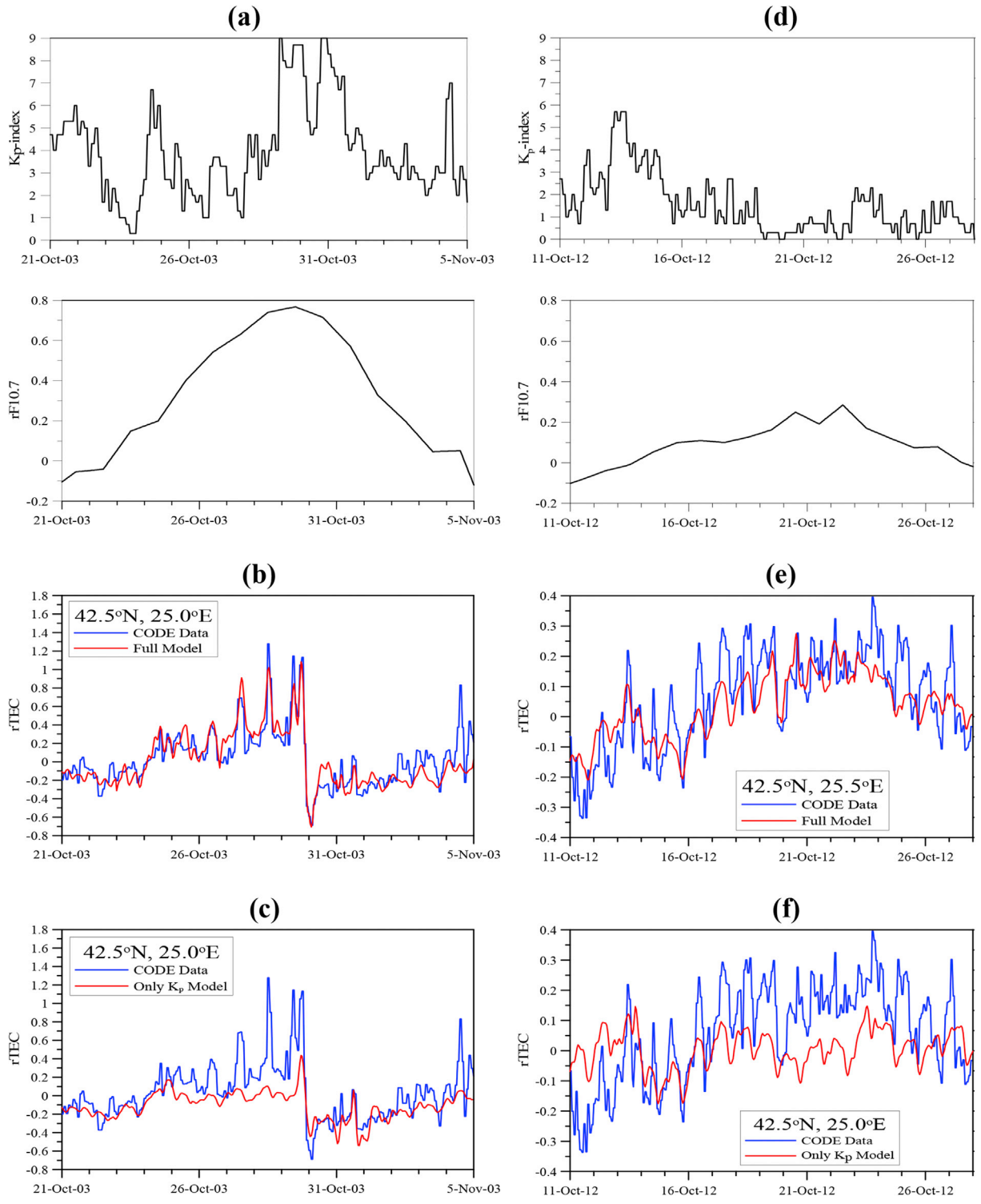

Fig. 12. **(a)** Temporal variability of the Kp-index (upper plot) and rF10.7 (second from above plot) for the period of 21 October-04 November 2003; **(b)** Comparison between the rTEC CODE data (blue line) and rTEC full model (red line), **(c)** The same as (b) but the only Kp model is used; both comparisons are for the period of time shown in (a); **(d), (e)** and **(f)** The same as (a), (b) and (c) respectively but for the period 11–27 October 2012. All comparisons are for the grid point (42.5°N, 25.0°E). (For interpretation of the references to colour in this figure legend, the reader is referred to the web version of this article.)

radiation (oscillations with period of solar rotation and its harmonics) described by the solar radio flux F10.7. The model is built on the basis of the CODE TEC data for full 17 years (January 1999–December 2015). It describes the most probable spatial distribution and temporal variability of the externally forced TEC anomalies assuming that they depend mainly on latitude, K_p-index, F10.7 and LT. The anomalies are expressed by the relative deviation of the TEC from its 15-day mean, as the mean value is calculated from the 15 preceding days. This means that the model predicts the correction to the 15-day mean values for each hour of the prediction period. The model offers rTEC and TEC values for 28 grid points; the area covered by the model is defined by: latitude from 35°N to 50°N with resolution of 2.5° and longitude from 15°E to 30°E with resolution of 5°. The predicted values depend on geographical coordinates, UT and date and are calculated for given/predicted K_p-index and F10.7.

The approach for building this regional model is similar to that reported by Andonov et al. (2011) constructed for North America or to the global model of Mukhtarov et al. (2013a). However this model includes an important improvement related to the short-term variability of the solar activity. This additional forcing has quite significant contribution to the ionosphere anomalies particularly during high and medium solar activity when day-to-day solar variations are large. This model includes also slightly improved geomagnetic forcing by using filtered values of the integrated K_p-index described in Section 4. In order to demonstrate the impact of the above mentioned two improvements on the model procedure we first evaluate the entire 2016 by calculating the systematic and *RMS* errors provided that these two improvements are excluded from the model, called here only K_p model; then we compare the obtained errors with the respective ones calculated from the full model and presented in Section 4. The systematic and *RMS* errors for 2016 calculated by using the only K_p model are respectively 0.142 TECU and 2.077 TECU. The both errors are larger than those (0.036 TECU and 1.889 TECU) obtained by using the full model. In order to demonstrate better the advantage of the full model with respect to the only K_p one we compare the longitude-latitude distributions of the *RMS* errors calculated by the two models for the period of 1999–2015. The comparison is shown in Fig. 5 where the (a) plot shows *RMS* distribution from the full model (it has been already shown before) while the (b) plot displays *RMS* distribution from the only K_p model. It is seen that while *RMS* errors from the full model change from 2.4 to 3.1 TECU those from the only K_p model change from 2.8 to 3.6 TECU. Hence on the average the full model decreases the *RMS* error by ~0.5 TECU.

In order to shed further light on the advantage of the full model with respect to the only K_p model we compare the rTEC anomalies driven by geomagnetic and short-term solar disturbances with different magnitudes; the results are shown in Fig. 12.

Fig. 12a shows the temporal variability of the K_p-index (upper plot) and *rF10.7* (bottom plot) for the period of 21 October-04 November 2003. It is seen that besides the large K_p-index disturbances particularly during the Halloween geomagnetic storms there is also a strong positive *rF10.7* anomaly with magnitude of ~0.8. Fig. 12b demonstrates the comparison between the rTEC CODE data (blue line) and rTEC full model (red line); the results are shown for the grid point (42.5°N, 25.0°E). Fig. 12c shows the same as (b) but when the only K_p model is used. This disturbed period clearly illustrates the superiority of the full model with respect to the only K_p one; Fig. 12c shows that not only most of the rTEC anomalies are not reproduced at all by the only K_p model but also the positive trend observed between 23 and 29 October in rTEC full model variability caused by the large *rF10.7* anomaly. This trend is stronger at the considered lowest latitude of 35°N; please, see the bottom plot of left column in Fig. 9. We note however that both models are not able to predict the rTEC anomalies seen on 04 November.

Fig. 12d displays the temporal variability of the K_p-index (upper plot) and *rF10.7* (bottom plot) for the period of 11–27 October 2012; the scales in Fig. 12a and d are the same. This period is characterized by a comparatively weak both K_p disturbance on October 13 and *rF10.7* anomaly with magnitude of ~0.3. Fig. 12e shows the comparison between the rTEC CODE data (blue line) and rTEC full model (red line) while Fig. 12f presents the same as (e) but when the only K_p model is used; the results are shown again for the grid point (42.5°N, 25.0°E). In this case the full model reproduces correctly the general rTEC variability defined mainly by the solar anomaly however underestimates the CODE rTEC data. The output of the only K_p model (Fig. 12f) however does not reproduce well the general data positive and then negative trends defined by the weak *rF10.7* anomaly; large differences can be seen particularly between 11 and 13 October when the modelled rTEC data overestimate the CODE data and between 19 and 25 October when he modelled rTEC data significantly underestimate the CODE data.

The capabilities of the regional model to predict the rTEC response to geomagnetic activity is demonstrated by considering three very strong geomagnetic storms; the Halloween storms on 29–30 October 2003 and the first two strongest storms of solar cycle 24 commenced on 17 March 2015 (St. Patrick's Day) and 22–23 June 2015. The comparison between the CODE and modelled TEC data are shown in Figs. 9–11 respectively. It has been already mentioned in the Introduction that Habarulema et al. (2010) evaluated the prediction capabilities of the NN model over South Africa for the Halloween storms period of 28–31 October 2003 and found that the *RMS* errors of this model changes between 3.45 and 6.61 TECU. According to Fig. 9c the RMS errors for the above mentioned period of the present model changes from 2.76 to 3.94 TECU, hence this model has better prediction capabilities than the NN model of Habarulema et al. (2010).

It is worth noting that this model might also be used operationally, i.e. for nowcasting and short-term prediction. For this purpose however a detailed validation of the model at different geophysical conditions has to be performed in order to clarify the model predicting performance. The geomagnetic storms in 2016 were however quite weak; the K_p-index was not larger than 6. The F10.7 day-to-day variations were also with small to medium amplitudes. It is worth noting that the prediction capability of this model depends not only on its predicting performance but on the predicted K_p-index and F10.7 as well. The short-term TEC prediction particularly during strong geomagnetic storms is a required task because it may improve the accuracy of the geodetic and navigation applications which have increasing importance for mitigating social and economic risks and for resolving some scientific problems.

Acknowledgement

We are grateful to the CODE TEC team for the access to the TEC data provided from the CODE FTP directory: ftp://ftp.unibe.ch/aiub/CODE/ and the Space Physics Interactive Data Resource (SPIDR), Boulder, Colorado. This work was supported by the European Office of Aerospace Research and Development (EOARD), Air Force Office of Scientific Research, Air Force Material Command, USAF, under grant number FA8655-12-1-2057 to D. Pancheva.

References

Andonov, B., Muhtarov, P., Kutiev, I., 2004. Analogue model, relating Kp index to solar wind parameters. J. Atmos. Sol.- Terr. Phys. 66, 927–932.

Andonov, B., Mukhtarov, P., Pancheva, D., 2011. Empirical model of the TEC response to the geomagnetic activity over the North American region. Adv. Space Res. 48, 1041–1048. https://doi.org/10.1016/j.asr.2011.05.007.

Astafyeva, E., Zakharenkova, I., Förster, M., 2015. Ionospheric response to the 2015 St. Patrick's Day storm: a global multi-instrumental overview. J. Geophys. Res. - Space Phys. 120, 9023–9037. https://doi.org/10.1002/2015JA021629.

Astafyeva, E., Zakharenkova, I., Alken, P., 2016. Prompt penetration electric fields and the extreme topside ionospheric response to the June 22–23, 2015 geomagnetic storm as seen by the Swarm constellation. Earth, Planets Space 68. https://doi.org/10.1186/s40623-016-0526-x, 152.

Balan, N., Yamamoto, M., Liu, J.Y., Otsuka, Y., Liu, H., Lühr, H., 2011. New aspects of thermospheric and ionospheric storms revealed by CHAMP. J. Geophys. Res. 116 https://doi.org/10.1029/2010JA016399. A07305.

Blagoveshchenskya, D.V., MacDougallb, J.W., Piatkova, A.V., 2006. Ionospheric effects preceding the October 2003 Halloween storm. J. Atmos. Sol.-Terr. Phys. 68, 821–831. https://doi.org/10.1016/j.jastp.2005.10.017.

Blanc, M., Richmond, A.D., 1980. The ionospheric disturbance dynamo. J. Geophys. Res. 85 (A4), 1669–1686. https://doi.org/10.1029/JA085iA04p01669.

Borries, C., Berdermann, J., Jakowski, N., Wilken, V., 2015. Ionospheric storms—a challenge for empirical forecast of the total electron content. J. Geophys. Res. - Space Phys. 120, 3175–3186. https://doi.org/10.1002/2015JA020988.

Buonsanto, M.J., 1999. Ionospheric storms – a review. Space Sci. Rev. 88, 563–601.

Feng, J., Wang, Z., Jiang, W., Zhao, Z., Zhang, B., 2016. A new regional total electron content empirical model in Northeast China. Adv. Space Res. 58, 1155–1167. https://doi.org/10.1016/j.asr.2016.06.001.

Fuller-Rowell, T.J., Codrescu, M.V., Moffett, R.J., Quegan, S., 1994. Response of the thermosphere and ionosphere to geomagnetic storms. J. Geophys. Res. 99, 3893–3914. https://doi.org/10.1029/93JA02015.

Habarulema, J.B., McKinnell, L.-A., Opperman, B.D.L., 2010. TEC measurements and modelling over Southern Africa during magnetic storms; a comparative analysis. J. Atmos. Sol. Terr. Phys. 72, 509–520. https://doi.org/10.1016/j.jastp.2010.01.012.

Habarulema, J.B., McKinnell, L.-A., Opperman, B.D.L., 2011. Regional GPS TEC modeling; Attempted spatial and temporal extrapolation of TEC using neural networks. J. Geophys. Res. 116 https://doi.org/10.1029/2010JA016269. A04314.

Heelis, R.A., Sojka, J.J., David, M., Schunk, R.W., 2009. Storm time density enhancements in the mid latitude dayside ionosphere. J. Geophys. Res. 114 https://doi.org/10.1029/2008JA013690. A03315.

Hernández-Pajares, M., Juan, J.M., Sanz, J., Orus, R., Garcia-Rigo, A., Feltens, J., Komjathy, A., Schaer, S.C., Krankowski, A., 2009. The IGS VTEC maps: a reliable source of ionospheric information since 1998. J. Geod. 83, 263–275. https://doi.org/10.1007/s00190-008-0266-1.

Huang, Z., Yuan, H., 2014. Ionospheric single-station TEC short-term forecast using RBF neural network. Radio Sci. 49 (4), 283–292. https://doi.org/10.1002/2013RS005247.

Jee, G., Lee, H.-B., Kim, Y.H., Chung, J.-K., Cho, J., 2010. Assessment of GPS global ionosphere maps (GIM) by comparison between CODE GIM and TOPEX/Jason TEC data: ionospheric perspective. J. Geophys. Res. 115 https://doi.org/10.1029/2010JA015432. A10319.

Kakinami, Y., Chen, C.H., Liu, J.Y., Oyama, K.-I., Yang, W.H., Abe, S., 2009. Empirical models of Total Electron Content based on functional fitting over Taiwan during geomagnetic quiet condition. Ann. Geophys. 27, 3321–3333.

Kamide, Y., Kusano, K., 2015. No major solar flares but the largest geomagnetic storm in the present solar cycle. Space weather 13, 365–367. https://doi.org/10.1002/2015SW001213.

Kelley, M.C., Vlasov, M.N., Foster, J.C., Coster, A.J., 2004. A quantitative explanation for the phenomenon known as storm-enhanced density. Geophys. Res. Lett. 31 https://doi.org/10.1029/2004GL020875. L19809.

Kutiev, I., Muhtarov, P., 2003. Empirical modeling of global ionospheric foF2 response to geomagnetic activity. J. Geophys. Res. 108 (A1), 1021,. https://doi.org/10.1029/2001JA009134.

Leandro, R.F., Santos, M.C., 2007. A neural network approach for regional vertical total electron content modelling. Stud. Geophys.et Geod. 51 (2), 279–292.

Lei, J., Wang, W., Burns, A.G., Yue, X., Dou, X., Luan, X., Solomon, S.C., Liu, Y.C.-M., 2014. New aspects of the ionospheric response to the October 2003 superstorms from multiple-satellite observations. J. Geophys. Res. Space Phys. 119, 2298–2317. https://doi.org/10.1002/2013JA019575.

Mannucci, A.J., Tsurutani, B.T., Ijima, B.A., Komjathy, A., Saito, A., Gonzalez, W.D., Guarnieri, F.L., Kozyra, U.J., Skoug, R., 2005. Dayside global ionospheric response to the major interplanetary events of October 29 – 30, 2003 “Halloween Storm’’. Geophys. Res. Lett. 32 https://doi.org/10.1029/2004GL021467. L12S02.

Mannucci, A.J., Tsurutani, B.T., Abdu, M.A., Gonzalez, W.D., Komjathy, A., Echer, E., Iijima, B.A., Crowley, G., Anderson, D., 2008. Superposed epoch analysis of the dayside ionospheric response to four intense geomagnetic storms. J. Geophys. Res. 113 https://doi.org/10.1029/2007JA012732. A00A02.

Mao, T., Wan, W., Yue, X., Sun, L., Zhao, B., Guo, J., 2008. An empirical orthogonal function model of total electron content over China. Radio Sci. 43 https://doi.org/10.1029/2007RS003629. RS2009.

Maruyama, T., 2007. Regional reference total electron content model over Japan based on neural network mapping techniques. Ann. Geophys. 25, 2609–2614.

Muhtarov, P., Kutiev, I., 1998. Empirical modeling of ionospheric storms at midlatitudes. Adv. Space Res. 22 (6), 829–835.

Muhtarov, P., Kutiev, I., Cander, L., 2002. Geomagnetically correlated autoregression model for short-term prediction of ionospheric parameters. Inverse Probl. 18, 49–65.

Mukhtarov, P., Andonov, B., Pancheva, D., 2013a. Global empirical model of TEC response to geomagnetic activity. J. Geophys. Res. 118, 6666–6685. https://doi.org/10.1002/jgra.50576.

Mukhtarov, P., Pancheva, D., Andonov, B., Pashova, L., 2013b. Global TEC maps based on the GNSS data: 1. Empirical background TEC model. J. Geophys. Res. 118 https://doi.org/10.1002/jgra.50413.

Nava, B., Rodríguez-Zuluaga, J., Alazo-Cuartas, K., Kashcheyev, A., Migoya-Orué, Y., Radicella, S.M., Amory-Mazaudier, C., Fleury, R., 2016. Middle- and low-latitude ionosphere response to 2015 St. Patrick's Day geomagnetic storm. J. Geophys. Res. - Space Phys. 121 https://doi.org/10.1002/2015JA022299.

Pancheva, D., Mukhtarov, P., Andonov, B., 2016. Global structure of ionospheric TEC anomalies driven by geomagnetic storms. J. Atmos. Sol.-Terr. Phys. 145, 170–182. https://doi.org/10.1016/j.jastp.2016.04.015.

Prölss, G.W., 1995. Ionospheric F-region storms. In: Volland, H. (Ed.), Handbook for Atmospheric Electrodynamics, V. 2. CRC Press, Boca Raton, pp. 195–248.

Prölss, G.W., 2005. Space weather effects in the upper atmosphere: low and middle latitudes. In: Scherer, K., Fichtner, H., Heber, B., Mall, U. (Eds.), Space Weather. Lecture Notes in Physics 656. Springer, Berlin, pp. 193–234.

Rishbeth, H., 1991. F-region storms and thermospheric dynamics. J. Geomag. Geoelectr. 43 (Suppl. l.), 513–524.

Rishbeth, H., 1998. How the thermospheric circulation affects the ionospheric F2-layer. J. Atmos. Terr. Phys. 60, 1385–1402.

Schaer, S., 1999. Mapping and Predicting the Earth's Ionosphere Using the Global Positioning System, Geod. Geophys. Arb. Schweiz., V. 59. Inst. für Geod. und Photogramm, Zurich, Switzerland.

Schunk, R.W., Nagy, A.F., 2000. Ionospheres: Physics, Plasma Physics, and Chemistry. Cambridge Univ. Press, New York.

Shepard, D., 1968. A Two-dimensional Interpolation Function for Irregularly-spaced Data. ACM ’68 Proc. ACM New York, NY, pp. 517–524. https://doi.org/10.1145/800186.810616.

Stankov, S.M., Kutiev, I.S., Jakowski, N., Wehrenpfennig, A., 2004. GPS TEC forecasting based on auto-correlation analysis. Acta Geod. geophys. hung. 39 (1), 1–14.

Tsurutani, B., et al., 2004. Global dayside ionospheric uplift and enhancement associated with interplanetary electric fields. J. Geophys. Res. 109 https://doi.org/10.1029/2003JA010342. A08302.

Tulunay, E., Senalp, E.T., Radicella, S.M., Tulunay, Y., 2006. Forecasting total electron content maps by neural network technique. Radio Sci. 41 https://doi.org/10.1029/2005RS003285. RS4016.

Yao, Y., Liu, L., Kong, J., Zhai, C., 2016. Analysis of the global ionospheric disturbances of the March 2015 great storm. J. Geophys. Res. 121, 12,157–12,170. https://doi.org/10.1002/2016JA023352.